Turbulence mitigation in a 28 GHz radio-over-free-space optics link using an integrated Mach-Zehnder interferometer and a diversity combining receiver

Dong-Nhat Nguyen [1*], Jan Bohata [1], Stanislav Zvanovec [1], Lim Nguyen [2], Zabih Ghassemlooy [3]

[1] Department of Electromagnetic Field, Czech Technical University in Prague, Prague, 166 27, Czech Republic
[2] Department of Electrical and Computer Engineering, University of Nebraska-Lincoln, Ohama, NE 68182, USA
[3] Optical Communications Research Group, Faculty of Engineering and Environment, Northumbria University, Newcastle upon Tyne, NE 1 8ST, UK
[*] dongnhat@fel.cvut.cz

Abstract: We propose an integrated Mach-Zehnder interferometer and diversity combining receiver (MZI-DC Rx) to mitigate the atmospheric turbulence-induced fading in millimetre-wave (MMW) radio-over-free-space optics (RoFSO) links. We have used a carrier frequency of 28 GHz as recommended for the fifth-generation wireless access networks and considered two optical MMW signal generation schemes namely double- and single-sidebands. In direct detection (DD)-based RoFSO, the link performance is limited by atmospheric turbulence. We show that, the proposed Rx can overcome this detrimental effect. It is verified by investigating the transmission of a 10 Gb/s 16-quadrature amplitude modulation signal at 28 GHz over a 1 km FSO channel under weak and strong turbulence regimes. For DSB-based MMW, the proposed Rx offers improved error vector magnitudes of about 0.8% and 5.7% and modulation error ratios of 1.3 and 4.9 dB under weak and strong turbulence regimes, respectively compared with the DD Rx. For the SSB scenario under weak turbulence, the proposed Rx achieves 4 dB improvement in receiver sensitivity and four orders of magnitude enhancement in the bit error rate over the DD Rx. The proposed Rx can be integrated on a single chip for further cost reduction.

1. Introduction

Transmission of radio frequency (RF) signals by means of an optical fibre (OF), known as radio-over-fibre (RoF), has been investigated for more than two decades to facilitate the wireless access to remote sites, cable television distribution and so on [1–3]. The future fifth-generation (5G) wireless networks, which provide data rate up to 10 Gb/s to users seamlessly, have been introduced using the frequency band of sub-6 GHz and 24 – 60 GHz. The latter millimetre-wave (MMW) band is more desirable and has received much attention for overcoming the high-speed transmission issue in 5G [4]. The frequency of 28 GHz, as part of the 26.5 – 29.5 GHz band, has already been adopted in Japan, South Korea, India and the US for commercial use [5]. This frequency band has also been demonstrated in RoF systems with the conventional direct detection (DD) receiver (Rx), i.e., using a single photodiode (PD) [6].

However, installation of OFs in RoF-based system can be time-consuming, costly and impractical particularly in urban and rural areas. Therefore, radio-over-free-space optics (RoFSO) has received much attention as an alternative to ensure the provision of high-speed wireless access to end users. Similar to OF communications, RoFSO technology offers a number of advantages including high-bandwidth, license-free, full-duplex operation, inherent security at the physical layer, low cost, easy deployment and re-use [7]. At present, commercially available FSO transceivers offer narrow beam divergence angle (i.e., of 0.55 mrad) with data rate and transmission distance up to 30 Gb/s and 1.5 km, respectively [8].

Fig. 1 shows the proposed deployment scenario of the RoFSO system in a common mobile fronthaul network where the central stations (CSs) within the backbone network acting as the gateway which can be connected to the base stations

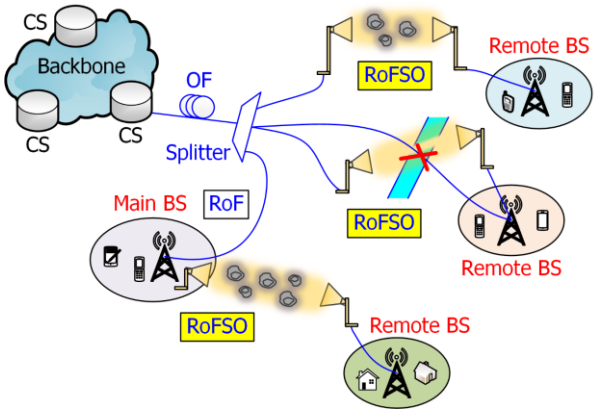

Fig. 1. Deployment of RoFSO systems for providing boradband wireless connectivity to remote and underserved areas. CS: central station, OF: optical fibre and BS: base station.

(BSs) via OFs. Seamlessly connected RoFSO with RoF features last-mile access applications and therefore extends broadband wireless access to remote and underserved areas [9]. In addition, this hybrid technology simplifies the fronthaul infrastructure with significant benefits to the service providers by centralizing some of the key modules such as MMW generation, switching and processing in the CS.

The optical beam propagating through the free-space channel is highly susceptible to atmospheric conditions, in particular the turbulence inducing due to temperature variations in the air [10], which results in the random phase and amplitude fluctuations of the optical signal. Recently, we demonstrated 100 MHz 64- quadrature amplitude modulation (QAM) transmission over 24 – 26 GHz RoFSO under turbulence using a conventional DD Rx [11], where we showed the dependency of the error vector magnitude (EVM)

on the turbulence level. For example, at a signal-to-noise ratio (SNR) of 22 dB, the measured EVMs were about 5% and 9% for the weak and strong turbulence regimes, respectively. To compensate for the deterioration of signal quality due to turbulence, a number of techniques have been proposed including transmit and receive diversity combining (DC) [12], modulation and coding [13] and adaptive threshold detection [14], to name a few. Very recently, we proposed and experimentally demonstrated the use of Mamyshev regenerator for turbulence mitigation in a 10 Gb/s return-to-zero (RZ) relay-assisted DD-based FSO transmission system [15]. We showed two orders of magnitude improvement in the bit error rate (BER) performance. Among these mitigation schemes, the DC-based Rx is considered as the most viable in terms of practical implementation and cost since it employs a PD array, which is commercially available. Note that, for DC-based schemes to be most effective, the multiple received signals should be somewhat uncorrelated. In FSO systems, the three most common linear combining techniques of maximal-ratio combining (MRC), equal-gain combining (EGC) and selection combining (SelC) have been investigated [14]. However, most of the works reported are theoretical in nature, with only a few reported at the system level. For example, in [16], we experimentally demonstrated 1 Mb/s non-return-to-zero (NRZ) baseband FSO links with SelC for transmission over two parallel lab-based turbulence channels of 5.5 m long but with only 0.9 m of partial correlation (i.e., intersecting the same turbulence area). This was a proof-of-concept, in order to simulate a real scenario where two links are terminated at the same point. Note, the SelC method is less complex since the received signals from two branches are sampled and the branch with the best signal quality is selected. In [17], 4 Gb/s 16-QAM for both uncorrelated FSO and MMW signals (i.e., within different channel state information) over the same free-space channel of 0.9 m under various synthesized weather conditions (fog and turbulence) was demonstrated. Following transmission, the measured EVM values for FSO and MMW signals were 17% and 9%, respectively. Using the higher complexity MRC algorithm, which was implemented offline, the EVM improved to 8.5% i.e., corresponding to the predicted SNR of 21.5 dB, for the hybrid FSO/MMW link.

In order to extend the range of OF transmission within the access networks, adaptive optical equalizers based on Mach-Zehnder interferometers (MZIs) have been proposed by Ozeki in 1992 [18] where single- and multiple-stage MZIs were reported. In 1994, Takiguchi *et al*. demonstrated a 5-stage MZI, which was fabricated on a planar lightwave circuit, for compensation of the fibre dispersion-induced distortion in a 2.5 Gb/s NRZ transmission system [19]. With the continuous development of a silicon photonic integrated circuit, in 2015 Dong *et al*. reported a fully-integrated chip composed of a MZI and an in-phase/quadrature modulator [20]. 50 Gb/s NRZ and 112 Gb/s 4-QAM transmissions were successfully demonstrated, as confirmed by the clear opening of the Rx eye diagram and constellation respectively that otherwise remained completely closed without the MZI chip. For example, at a BER of 2.4×10^{-2}, the MZI resulted in about 2.5 dB improvement in the optical SNR for 4-QAM. 25 and 50 Gb/s links with the duobinary signal in DD-based optical access networks using 1st and 2nd orders optical pre-equalizers for OF dispersion compensation was also reported in [21]. In this paper, for the first time, we propose an integrated single-stage MZI-DC Rx, which circumvents the implementation difficulty while mitigating more effectively the turbulence effects in a unique way. We investigate the performance of MZI-DC Rx to alleviate the turbulence-induced fading transmission of the RF 16-QAM signal over a 1 km distance FSO. We have used the 5G frequency of 28 GHz, which has not been reported yet in the literature for RoFSO system. Two optical MMW signal generation schemes are considered, namely double-sideband (DSB) and single-sideband (SSB). In DSB, two laser outputs are modulated at CS, whereas in SSB only a single laser output is externally modulated and optically combined with the unmodulated carrier. Performance comparison of DSB and SSB schemes have been reported for a 155 Mb/s NRZ RoF link with a self-homodyne based Rx [22]. However, no direct performance comparison between DSB and SSB in RoFSO systems has been reported yet. Thus, the main contributions of this paper can be summarized as follows:

1) Investigation of weak and strong turbulence regimes (based on outdoor turbulence measurements in the Czech Republic) impact on a 10 Gb/s 16-QAM optical heterodyning-based 28 GHz RoFSO link with DSB and SSB schemes.

2) Evaluation of the proposed MZI-DC Rx, which can be integrated and fabricated in a single chip, for adaptive turbulence mitigation and comprehensive comparison with the conventional DD Rx in terms of the EVM, MER, BER, power penalty and constellation diagrams.

The rest of the paper is organized as follows: Section 2 describes the system configurations with a brief theoretical analysis. Section 3 presents the simulation results and discusses the performance of 16-QAM for DSB- and SSB-based RoFSO configurations when using the proposed Rx. Lastly, Section 4 summarizes the paper.

2. 28 GHz RoFSO system using MZI-DC Rx

Fig. 2 displays the simulation setup of the optical heterodyning-based RoFSO with the MZI-DC Rx for turbulence mitigation. At the transmitter (Tx), two continuous-wave lasers operating at 1552.524 and 1552.299 nm were heterodyned via an optical combiner to generate a 28 GHz DSB MMW carrier frequency. Polarization controllers (PC) were used to minimize the polarization-dependent loss. The combined optical carriers were then modulated with a 10 Gb/s 16-QAM-based orthogonal frequency-division-multiplexing data signal using a single-drive MZM. A signal with a total bandwidth of 2.5 GHz modulated at the frequency of 7.5 GHz is shown in the inset (i). The 16-QAM signal was amplified by an electrical amplifier (EA) to a level of about 6 dBm as in experiments [23]. The 16-QAM modulated optical carrier signal is depicted in the inset (ii). The output of MZM with a power level of 2.5 dBm was launched into a 1 km free-space channel using an FSO Tx [8].

In this work, we only consider weak to strong turbulence regimes, which is best modelled by the Gamma-Gamma (ΓΓ) distribution as given in [24]. For turbulence, the

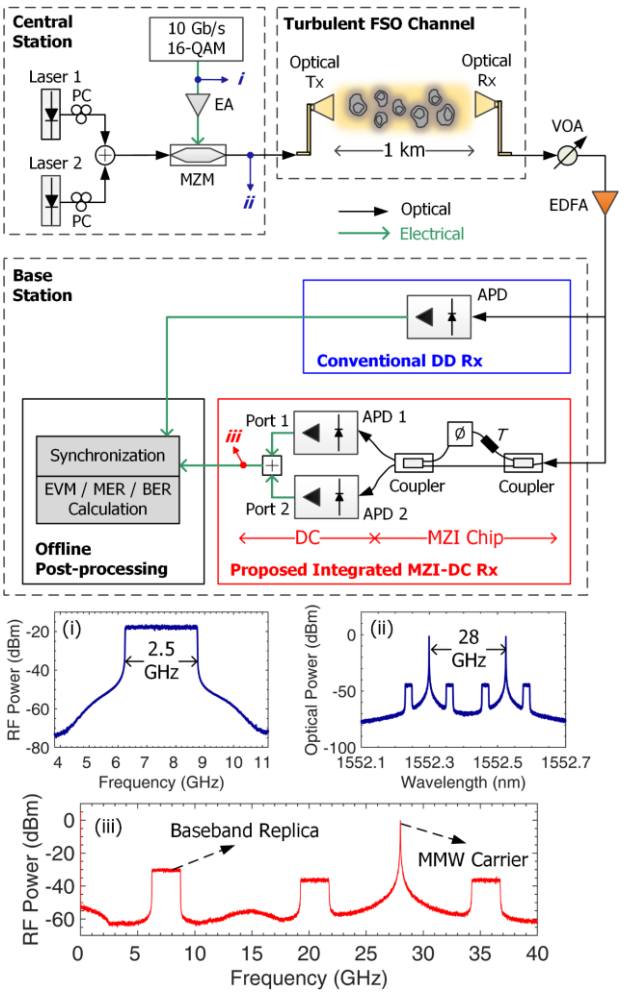

Fig. 2. Simulation setup of the MZI-DC Rx for turbulence mitigation. EA: electrical amplifier, PC: polarizaion controller, MZM: Mach-Zehnder modulator, VOA: variable optical attenuator, EDFA: erbium-doped fibre amplifier and APD: avalanche photodiode. Insets (i), (ii) and (iii) depict the optical and RF spectra at respective locations ***i***, ***ii*** and ***iii***.

key parameter is the refractive index structure parameter C_n^2 ($m^{-2/3}$), which can be obtained from the Rytov variance, given by [24]:

$$\sigma_R^2 = 1.23 C_n^2 k^{7/6} L^{11/6}\,, \tag{1}$$

$$C_n^2 = \left(86 \times 10^{-6} \frac{P}{T^2}\right)^2 C_T^2\,, \tag{2}$$

where $k = 2\pi/\lambda$ is the wave number and L is the free-space propagation distance (1 km in our case). P is the atmospheric pressure in millibar, T is the absolute temperature in Kelvin and C_T^2 is the temperature structure parameter defined as [24]:

$$C_T^2 = (T_1 - T_2)^2 / d^{2/3}. \tag{3}$$

where T_1 and T_2 are temperatures at two points separated by distance d.

σ_R^2 is commonly used to classify turbulence regimes of weak ($\sigma_R^2 < 1$), moderate ($\sigma_R^2 = 1$) and strong ($\sigma_R^2 > 1$) [24]. Note, C_n^2 of 1.3×10^{-16} $m^{-2/3}$ and 5×10^{-13} $m^{-2/3}$ correspond to Rytov variances of 0.0026 and 9.9548, respectively are considered in this work to represent weak and strong turbulence levels accordingly. The C_n^2 values are

Table 1. Key parameters used in simulation.

Parameter	Value
Laser: Wavelengths and power	1552.524 and 1552.299 nm, and 10 dBm
Carrier frequency	28 GHz
Modulation format (data rate)	16-QAM (10 Gb/s)
FSO • Tx/Rx aperture • Beam divergence • Distance • Weak turbulence • Strong turbulence	 10 cm 0.55 mrad 1 km 1.3×10^{-16} $m^{-2/3}$ 5×10^{-13} $m^{-2/3}$
EDFA: Gain and noise figure	20 dB and 3 dB
APD: Responsivity and dark current	0.65 A/W and 10 nA
TIA gain	22 dB

equivalent to the real-time outdoor measurements, which were carried out during Summer 2011 in Prague, Czech Republic [25].

At the Rx, a variable optical attenuator (VOA) adjusted the received optical power (P_r) levels. The signal was then boosted using an erbium-doped fibre amplifier (EDFA). It is anticipated that, practical systems in 5G fronthaul will employ an EDFA, which will share the same optical infrastructure of current access networks, e.g., passive optical networks [23]. The optically amplified signal was coupled into the proposed Rx, which is composed of a single-stage MZI chip and the DC Rx. The MZI structure consists of two 2×2 optical couplers with coupling coefficients of 0.5. One arm is composed of relative optical path delay T and phase shifter ϕ. The frequency response of MZI is given by [26]:

$$H(\omega) = 1 + \exp\{i(\omega T + \phi)\}. \tag{4}$$

T and ϕ should be adjusted to minimize the BER. In particular, T should be shorter than the bit duration at a certain bit rate for the optimum performance [26]. MZI with tunable parameters can be used as an adaptive optical equalizer. Detailed optimization of MZI will be given later.

The DC stage is composed of two optical Rxs (i.e., two avalanche photodiodes (APDs) and transimpedance amplifiers (TIAs)) and a combiner to realize EGC. Note, EGC is much simpler to implement than MRC since it requires no instantaneous channel state information. Note that, state-of-the-art commercial APD show improved sensitivity (by up to 12 dB) compared with the PIN PD as reported in [27, 28], thus ensuring a sufficient link power budget for serving a higher number of users. In [29], an integrated APD and TIA fabricated in a silicon platform was reported for a 40 Gb/s OF link. Therefore, it should be possible to fabricate the proposed MZI-DC Rx in a single chip in the near future.

The combined MMW signal is shown in the inset (iii) with the baseband replica confirming the successful transmission and recovery of 10 Gb/s 16-QAM. To assess the

link performance, we have used three standard quality metrics, EVM, modulation error ratio (MER) and BER commonly used in evaluating RoFSO systems [30]. We estimated the root mean square EVM for signal constellations consisting of more than 30,000 symbols. A measure of SNR is given by MER = $(I_r^2 + Q_r^2)/\{(I_r - I_o)^2 + (Q_r - Q_o)^2\}$, where I_r, Q_r are the demodulated in-phase and quadrature-phase components of QAM and I_o and Q_o are the ideal normalized in-phase and quadrature-phase components, respectively. We have used constellation diagrams to compare the performance of the proposed MZI-DC Rx with the conventional DD Rx, which is also illustrated in Fig. 2. Table 1 summarizes the main system parameters.

3. Simulation results and discussion

3.1 Transmission performance of 10 Gb/s DSB 16-QAM under weak turbulence

Prior to evaluating the transmission performance of the system with the proposed Rx, first we need to select optimum T and ϕ for the MZI chip. Note, we have set ϕ to 0° and T is swept at 1 ps interval over a full bit period of 100 ps. Fig. 3(a) depicts the EVM as a function of T, which shows that increasing T results in a rotation of constellations with increased noise levels, thus leading to phase errors and significantly higher EVM values. For example, for T = 12 ps, the EVM is about 24.3%, which is above the required limit of 12.5% for 16-QAM as specified in the third generation partnership project (3GPP) [31]. For T < 6 ps, the EVM meets the 12.5% EVM requirement. The lowest EVM of 5% was achieved for T = 1 ps. With selected T = 1 ps in this work, we then swept ϕ for further EVM analysis. The plot of EVM versus ϕ is illustrated in Fig. 3(b), which displays a symmetrical profile around ϕ = 180°. The highest EVM of ~19%, which is above the required limit, is observed at ϕ of 80° and 280°. The constellation diagrams also demonstrate the impact of higher ϕ on the link performance, with more stable constellations are observed at EVM of 5%. For ϕ within the ranges of 0° – 40°, 160° – 200° and 320° – 360°, the EVM values are below 6% with the lowest EVM of 5% at ϕ of 0° and 360°. For a fair comparison in all simulation scenarios, we have selected ϕ = 5°.

Fig. 4 shows the simulated EVM and MER performance of 10 Gb/s DSB 16-QAM for a 1 km FSO transmission link under weak turbulence (C_n^2 = 1.3×10^{-16} m$^{-2/3}$) with the conventional DD and MZI-DC Rx. Also shown is the 12.5% limit. Overall, the proposed Rx improves the link performance to a certain degree, especially at low values of P_r. In particular, at P_r of -16 dBm, the EVM and MER values are 5.8% and 24.5 dB for the DD Rx, respectively. The proposed MZI-DC Rx improves the EVM and MER performance by 0.8% and 1.3 dB, respectively. At lower values of P_r, e.g., -26 dBm, for the DD Rx the EVM of 14.7% is above the 12.5% limit, whereas for the proposed Rx it is ~ 12%, i.e. just below the limit. Note that, for the proposed MZI-DC Rx, the EVM is reduced by ~10% compared with ~14% for the DD Rx for the range of P_r.

To illustrate the EVM performance improvement using the MZI-DC Rx, we first performed simulations (under weak turbulence) for each output port of the MZI chip (ports 1 and 2 in Fig. 2) with no DC, which is used as the baseline for each detector. The results are shown in Fig. 5, where the

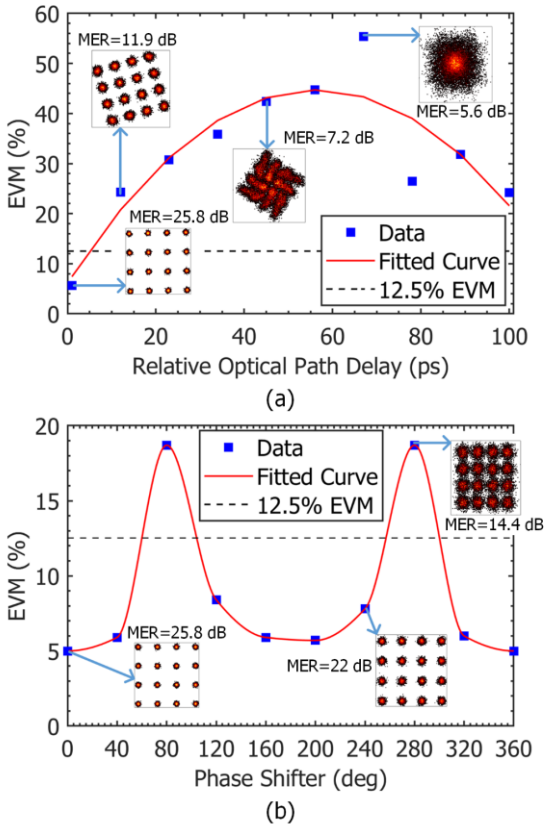

Fig. 3. EVM performance obtained with different values of: (a) relative optical path delay T and (b) phase shifter ϕ of the MZI for T = 1 ps. Insets are the received constellation diagrams.

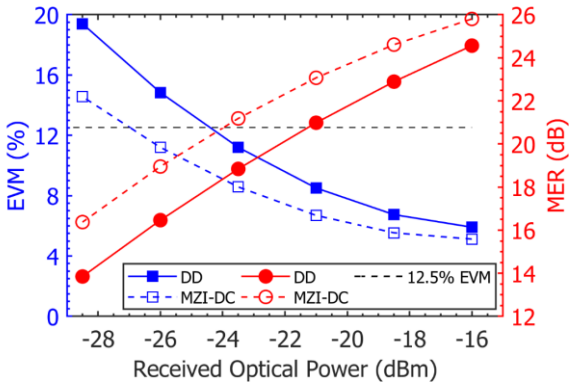

Fig. 4. EVM and MER performance of 10 Gb/s DSB 16-QAM as a function of P_r for transmisison over a 1 km FSO link under weak turbulence (C_n^2 = 1.3×10^{-16} m$^{-2/3}$). Square and circle symbols denote EVM and MER performance, respectively.

EVM plot is well above the EVM limit of 12.5% for port 1 and reaching the EVM floor of ~36% for all values of P_r whereas for the port 2 the plot is below the EVM limit for P_r > - 26 dBm. Note that, port 2 also outperforms the DD Rx, see Fig. 4, in terms of EVM by ~2.9% at P_r of -26 dBm. This improvement is because of the MZI chip, which acts as a two-tap optical equalizer for increasing the modulation bandwidth [20], reshaping the signal by suppressing the unwanted frequency components on the sidelobes and reducing the noise floor level [21]. The constellation diagrams of 10 Gb/s 16-QAM at P_r of -26 dBm for the DD and MZI-DC Rxs are shown in Fig. 6 for quantitative comparison. For the case of port 1 being active (port 2 OFF) the symbols are completely

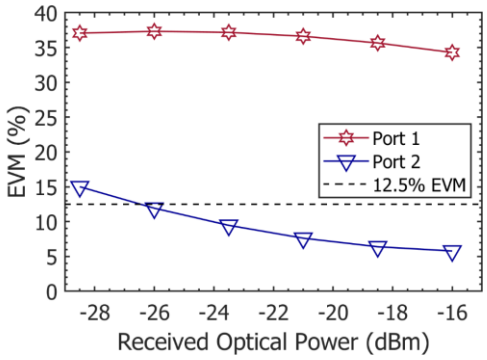

Fig. 5. EVM performance of 10 Gb/s 16-QAM signal as a function of P_r after transmisison over 1 km FSO link under weak turbulence with each port of the MZI chip (i.e., single detector, no DC).

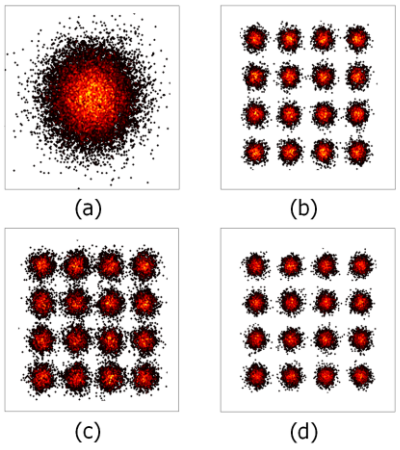

Fig. 6. Constellation diagrams of 10 Gb/s 16-QAM signal obtained at P_r of -26 dBm with: (a) single detector (Port 1 active only), (b) single detector (Port 2 active only), (c) conventional DD Rx and (d) combined port.

smeared, see Fig. 6(a), which correspond to EVM and MER values of 36.9% and 7.8 dB, respectively. A clearer constellation is shown in Fig. 6(b) for only port 2 being ON (port 1 OFF), achieving an EVM of 11.8% (below the required limit) and MER of 18.3 dB.

The proposed Rx takes advantage of the correlation between the two ports by employing DC with EGC to further mitigate turbulence and improve the link reliability. For the combined port, the constellation diagram for EVM and MER of 11% and 18.9 dB, respectively shown in Fig. 6(d) is superior and more stable than the DD Rx, see Fig. 6(c).

3.2 Transmission performance of 10 Gb/s DSB 16-QAM under strong turbulence

Fig. 7 depicts the EVM and MER performance as a function of P_r for both the proposed and DD Rxs under strong turbulence (i.e., $C_n^2 = 5\times10^{-13}$ m$^{-2/3}$). As shown, the DD Rx displays the worst EVM and MER performance compared with the MZI-DC Rx. For instance, at P_r of -20 dBm, the EVM and MER gains for MZI-DC Rx are 5.7% and 4.9 dB, respectively, compared with the DD Rx. Note, higher MER corresponds to less scattering observed in the constellation diagrams, thus improved symbol errors, see Fig. 8. The

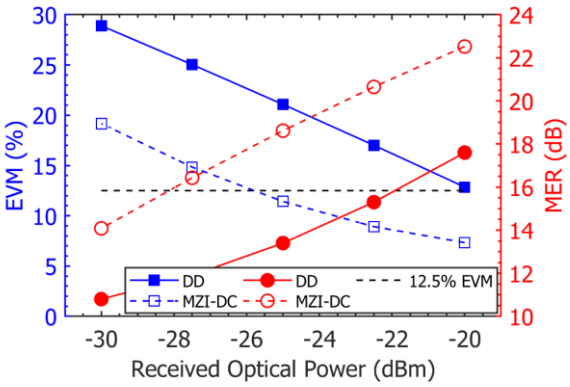

Fig. 7. EVM and MER performance of 10 Gb/s DSB 16-QAM as a function of P_r for a 1 km FSO link under strong turbulence ($C_n^2 = 5\times10^{-13}$ m$^{-2/3}$). Square and circle symbols denote EVM and MER performance, respectively.

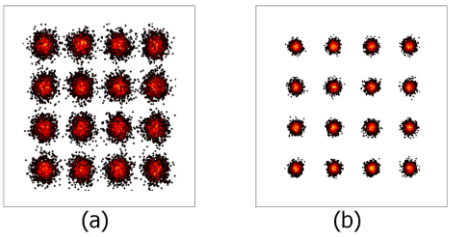

Fig. 8. Constellation diagrams of 10 Gb/s 16-QAM at P_r of -20 dBm for a 1 km FSO link under strong turbulence with: (a) conventional DD Rx and (b) MZI-DC Rx.

results confirm that the MZI-DC Rx is more effective in mitigating strong turbulence.

We further verify the effectiveness of the MZI-DC Rx by evaluating the BER performance of the 28 GHz DSB 16-QAM RoFSO link. The BER for M-QAM is given by:

$$\mathrm{BER}_{M-\mathrm{QAM}} = \frac{2}{\boldsymbol{log_2(M)}}\left(1-\frac{1}{\sqrt{M}}\right)\times \ \mathrm{erfc}\left(\sqrt{\frac{3}{2(M-1)}\times\frac{1}{\mathrm{EVM}^2}}\right). \quad (5)$$

where erfc (·) is the complementary error function [9].

Figs. 9(a) and (b) display the BER performance of 10 Gb/s DSB 16-QAM as a function of P_r for a 1 km FSO transmission link under weak and strong turbulence regimes, respectively for both Rxs. Also shown is Reed-Solomon (255, 239) forward error correction (FEC) limit of 2×10^{-4}, which is commonly adopted in RoFSO systems [30]. As can be seen, the MZI-DC Rx outperforms the DD Rx. For example, at the FEC criterion for MZI-DC Rx the power gains are about 2.5 and 7 dB for the weak and strong turbulence regimes, respectively compared with the DD Rx. Table 2 summarizes the performance results for BER, EVM and MER for 28 GHz RoFSO with 10 Gb/s DSB 16-QAM under the weak and strong turbulence regimes. Note, the BER values lower than 10^{-12} is considered error-free transmission [3].

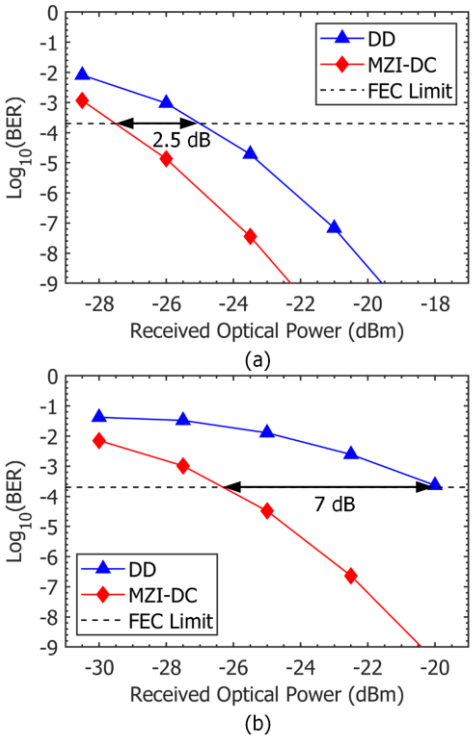

Fig. 9. BER performance of 10 Gb/s DSB 16-QAM as a function of P_r after transmisison over 1 km FSO link under: (a) weak and (b) strong turbulence.

Table 2. Summary of transmission results of 10 Gb/s DSB 16-QAM in 28 GHz RoFSO system using conventional DD and proposed MZI-DC Rx.

Turbulence level	DD Rx			MZI-DC Rx		
	EVM (%)	MER (dB)	BER	EVM (%)	MER (dB)	BER
Weak	5.8	24.5	$<10^{-12}$	5	25.8	$<10^{-12}$
Strong	13	17.6	2×10^{-4}	7.3	22.5	3×10^{-10}

3.3 Transmission performance of 10 Gb/s SSB 16-QAM under weak turbulence

In this section, the application of the MZI-DC Rx in SSB 28 GHz RoFSO is presented. As shown in Fig. 10(a), laser 1 is externally modulated by 10 Gb/s 16-QAM prior to being combined with the output of unmodulated laser 2. The optical spectrum featuring the SSB is depicted in Fig. 10(b). The optical power launched into the free space-channel is kept at 2.5 dBm for a fair comparison with DSB. Note, the rest of the setups used are the same as those outlined in Section 2. However for simplicity, only weak turbulence ($C_n^2 = 1.3\times10^{-16}$ $m^{-2/3}$) is considered.

Fig. 11 shows the simulated EVM and MER performance of 10 Gb/s SSB 16-QAM following transmission over a 1 km free-space channel under weak turbulence for the DD- and MZI-DC-based Rxs. As expected, the proposed MZI-DC Rx outperforms the conventional DD Rx, achieving a 4 dB power gain at the 12.5 % EVM requirement. For P_r of -16 dBm, the proposed MZI-DC Rx

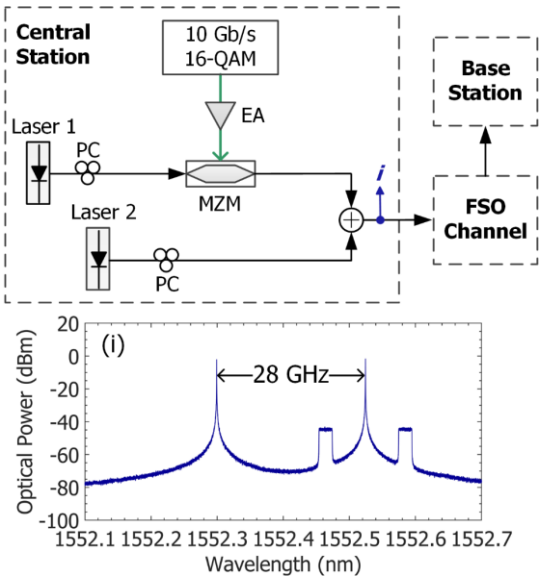

Fig. 10. 10 Gb/s SSB 16-QAM RoFSO transmisison block diagram. Inset (i) depicts the optical spectrum at respective location ***i***.

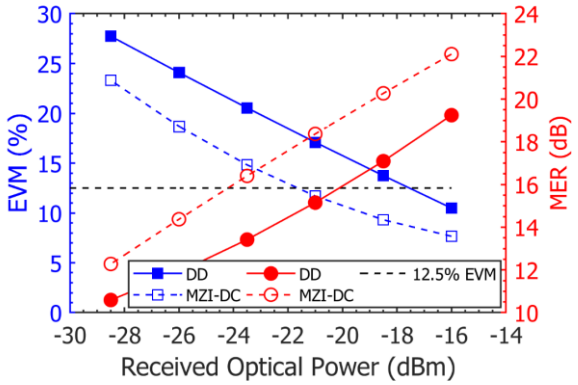

Fig. 11. EVM and MER performance of 10 Gb/s SSB 16-QAM as a function of P_r after transmisison over a 1 km FSO link under weak turbulence ($C_n^2 = 1.3\times10^{-16}$ $m^{-2/3}$). Square and circle symbols denote EVM and MER performance, respectively.

achieves improved EVM and MER performance by 6.7% and 3.6 dB, respectively compared with the DD Rx.

We also confirm the effectiveness of the proposed MZI-DC Rx for the system with SSB by computing the BERs and constellations as displayed in Fig. 12. With weak turbulence and at the FEC limit, the power penalty for DD Rx is 4 dB compared with the SSB MZI-DC Rx. The improvement in the signal quality can also be observed from the constellation diagrams captured at P_r of -16 dBm, shown by the insets. For the DD Rx, we could clearly observe in inset (i) the impairments on the constellation symbols caused by turbulence, thus resulting in higher BER (i.e., 1.1×10^{-5}). In the SSB MZI-DC Rx, the constellation is more stable for a lower BER of 2.4×10^{-9}. However, compared with the DSB results in Fig. 9(a), SSB is inferior by almost 5 dB at the FEC limit, which is in line with previously reported experimental results for 155 Mb/s NRZ optical heterodyning-based RoF link [22].

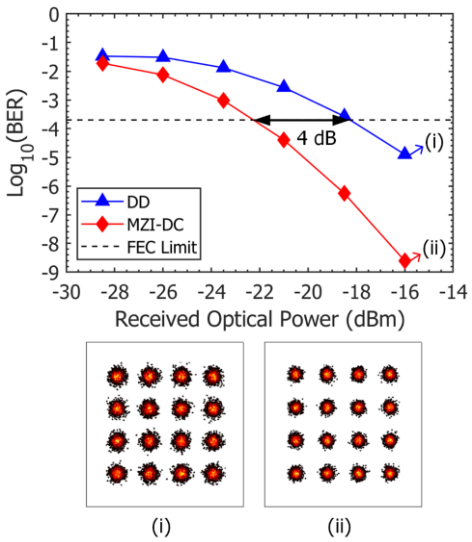

Fig. 12. BER performance of 10 Gb/s SSB 16-QAM as a function of P_r after transmisison over a 1 km FSO link under weak turbulence. Insets are 16-QAM constellations obtained at P_r of -16 dBm for (i) conventional DD Rx and (ii) MZI-DC Rx.

4. Conclusions

We proposed an integrated Mach-Zehnder interferometer and diversity combining receiver for adaptive turbulence mitigation in optical heterodyning-based DSB and SSB 28 GHz RoFSO systems using 16-QAM. The proposed Rx holds promise to further extend the FSO transmission distance for reliable last-mile applications, thereby providing broadband service to remote areas. The results showed that, after 1 km FSO transmission under weak and strong turbulence levels, the proposed MZI-DC Rx consistently outperformed the conventional direct detection Rx in terms of EVM, MER and BER. We showed that the proposed Rx offered the followings: (i) receiver sensitivity gains of 2.5 and 4 dB for DSB and SSB schemes, respectively compared with the conventional DD Rx under weak turbulence and at the FEC limit; (ii) improved sensitivity of about 7 dB for DSB under strong turbulence; and (iii) the potential of being integrated on a single chip for further cost reduction. It is anticipated that, the proposed Rx will also be able to adaptively mitigate turbulence in RoFSO systems using different modulation formats and frequency bands, which will be part of our future works.

5. Acknowledgements

This work was supported by International Mobility of Researchers in CTU (CZ.02.2.69/0.0/0.0/16_027/0008465) and MEYS INTERCOST project LTC18008 within COST CA16220.

6. References

1 Smith, G.H., Novak, D., Ahmed, Z.: 'Overcoming chromatic-dispersion effects in fiber-wireless systems incorporating external modulators'*IEEE Trans. Microw. Theory Tech.*, 1997, **45**, (8), pp. 1410–1415.

2 Thomas, V.A., El-Hajjar, M., Hanzo, L.: 'Optical single sideband signal generation relying on a single-drive Mach-Zehnder modulator for radio over fibre communications'*IET Commun.*, 2016, **10**, (5), pp. 534–539.

3 Novak, D., Waterhouse, R.B., Nirmalathas, A., *et al.*: 'Radio-over-fiber technologies for emerging wireless systems'*IEEE J. Quantum Electron.*, 2016, **52**, (1), pp. 1–11.

4 Rappaport, T.S., Xing, Y., MacCartney, G.R., Molisch, A.F., Mellios, E., Zhang, J.: 'Overview of millimeter wave communications for fifth-generation (5G) wireless networks-with a focus on propagation models'*IEEE Trans. Antennas Propag.*, 2017, **65**, (12), pp. 6213–6230.

5 '5G spectrum GSMA public policy position', https://www.gsma.com/

6 Van Kerrebrouck, J., Li, H., Spiga, S., *et al.*: '10 Gb/s radio-over-fiber at 28 GHz carrier frequency link based on 1550 nm VCSEL chirp enhanced intensity modulation after 2 km fiber'*2018 Opt. Fiber Commun. Conf. Expo.*, 2018, p. W1F.1.

7 Pernice, R., Andò, A., Cardinale, M., *et al.*: 'Indoor free space optics link under the weak turbulence regime: measurements and model validation'*IET Commun.*, 2015, **9**, (1), pp. 62–70.

8 'Free space optics 10 gigabits EL-10G', http://www.ecsystem.cz

9 Nguyen, D.-N., Bohata, J., Spacil, J., *et al.*: 'M-QAM transmission over hybrid microwave photonic links at the K-band'*Opt. Express*, 2019, **27**, (23), p. 33745.

10 Ghassemlooy, Z., Popoola, W.O., Rajbhandari, S.: 'Optical wireless communications – system and channel modelling with Matlab' (CRC Press, 2019, 2nd edn.)

11 Bohata, J., Komanec, M., Spáčil, J., Ghassemlooy, Z., Zvánovec, S., Slavík, R.: '24–26 GHz radio-over-fiber and free-space optics for fifth-generation systems'*Opt. Lett.*, 2018, **43**, (5), pp. 1035–1038.

12 Rakia, T., Yang, H.C., Alouini, M.S., Gebali, F.: 'Outage analysis of practical FSO/RF hybrid system with adaptive combining'*IEEE Commun. Lett.*, 2015, **19**, (8), pp. 1366–1369.

13 Kaushal, H., Kaddoum, G.: 'Optical communication in space: challenges and mitigation techniques'*IEEE Commun. Surv. Tutorials*, 2017, **19**, (1), pp. 57–96.

14 Khalighi, M.A., Uysal, M.: 'Survey on free space optical communication: a communication theory perspective'*IEEE Commun. Surv. Tutorials*, 2014, **16**, (4), pp. 2231–2258.

15 Nor, N.A.M., Komanec, M., Bohata, J., Ghassemlooy, Z., Bhatnagar, M.R., Zvánovec, S.: 'Experimental all-optical relay-assisted FSO link with regeneration and forward scheme for ultra-short pulse transmission'*Opt. Express*, 2019, **27**, (16), p. 22127.

16 Zvanovec, S., Perez, J., Ghassemlooy, Z., Rajbhandari, S., Libich, J.: 'Route diversity analyses for free-space optical wireless links within turbulent scenarios.'*Opt. Express*, 2013, **21**, (6), pp. 7641–50.

17 Zhang, J., Wang, J., Xu, Y., *et al.*: 'Fiber–wireless integrated mobile backhaul network based on a hybrid millimeter-wave and free-space-optics architecture with an adaptive diversity combining technique'*Opt. Lett.*, 2016, **41**, (9), p. 1909.

18 Ozeki, T.: 'Optical equalizers'*Opt. Lett.*, 1992, **17**, (5), p. 375.

19 Takiguchi, K., Okamoto, K., Moriwaki, K.: 'Dispersion compensation using a planar lightwave circuit optical equalizer'*IEEE Photonics Technol. Lett.*, 1994, **6**, (4), pp. 561–564.

20 Dong, P., Xie, C., Buhl, L.L., Chen, Y.-K., Sinsky, J.H., Raybon, G.: 'Silicon in-phase/quadrature modulator with on-chip optical equalizer'*J. Lightwave Technol.*, 2015, **33**, (6), pp. 1191–1196.

21 Dong-Nhat, N., Nguyen, L., Malekmohammadi, A.: 'Using duobinary with first- and second-order optical equalisers for extending transmission distance of optical access networks'*IET Optoelectron.*, 2018, **12**, (5), pp. 239–243.

22 Islam, A.H.M.R., Bakaul, M., Nirmalathas, A., Town, G.E.:

'Simplification of millimeter-wave radio-over-fiber system employing heterodyning of uncorrelated optical carriers and self-homodyning of RF signal at the receiver'*Opt. Express*, 2012, **20**, (5), p. 5707.

23 Dat, P.T., Kanno, A., Inagaki, K., Kawanishi, T.: 'High-capacity wireless backhaul network using seamless convergence of radio-over-fiber'*J. Lightwave Technol.*, 2014, **32**, (20), pp. 3910–3923.

24 Andrews, L.C., Phillips, R.L.: 'Laser beam propagation through random media' (SPIE, 2005)

25 Grabner, M., Kvicera, V.: 'Measurement of the structure constant of refractivity at optical wavelengths using a scintillometer'*Radioengineering*, 2012, **21**, (1), pp. 455–458.

26 Doerr, C.R., Chandrasekhar, S., Winzer, P.J., *et al.*: 'Simple multichannel optical equalizer for mitigating intersymbol interference for 40-Gb/s nonreturn-to-zero signals'*J. Lightwave Technol.*, 2004, **22**, (1), pp. 249–256.

27 Hsu, J.-H., Yu, M., Liu, F., *et al.*: 'On channel estimation schemes for APD-based DDM-OFDM-PONs under sub-Nyquist sampling'*Opt. Express*, 2018, **26**, (18), p. 23808.

28 Houtsma, V., Veen, D. Van: 'Bi-directional 25G/50G TDM-PON with extended power budget using 25G APD and coherent detection'*J. Lightwave Technol.*, 2018, **36**, (1), pp. 122–127.

29 Verbist, J., Lambrecht, J., Moeneclaey, B., *et al.*: '40-Gb/s PAM-4 transmission over a 40 km amplifier-less link using a sub-5V Ge APD'*Photonics Technol. Lett.*, 2017, **29**, (24), pp. 2238–2241.

30 Naila, C. Ben, Wakamori, K., Matsumoto, M., Bekkali, A., Tsukamoto, K.: 'Transmission analysis of digital TV signals over a radio-on-FSO channel'*IEEE Commun. Mag.*, 2012, **50**, (8), pp. 137–144.

31 36.104, 3GPP TS: 'Base station (BS) radio transmission and reception' (2018)